International Journal of Thermophysics, Vol. 21, No. 6, 2000

Transient Hot Wire (THW) Method: Uncertainty Assessment

U. Hammerschmidt[1,2] and W. Sabuga[1]

Received May 3, 2000

The standard method for measuring thermal transport properties of dielectric solids such as ceramics and refractories is the transient hot wire (THW) technique. In its simplest arrangement, a thin wire is embedded between two sample halves, where it acts simultaneously as a resistive heat source and a thermometer. From its temperature signal, the thermal conductivity and the thermal diffusivity of the dielectric can be derived. Up to now, there is no uncertainty assessment for this technique strictly following the ISO Guide to the Expression of Uncertainty in Measurement. Here we analyze the ISO standard uncertainty of the THW technique in the same way as in a previous paper on the uncertainty of the closely related transient hot strip (THS) technique. The two papers provide a comprehensive comparison of the most important advantages and disadvantages of these two transient techniques. The results obtained here for the uncertainty (5.8% for the thermal conductivity and 30% for the thermal diffusivity) are nearly the same as those for the THS method. Experiments on a Pyrex standard-reference sample confirm the results.

KEY WORDS: standard uncertainty; thermal conductivity; thermal diffusivity; transient hot strip method; transient hot wire method.

1. INTRODUCTION

Among the non-steady-state techniques to measure the thermal conductivity λ and thermal diffusivity a of dielectric solids, the transient hot wire (THW) method is by far the most frequently used (e.g., Refs. 1–5). In practice, there are three different experimental arrangements: the standard one-wire setup and two modified versions, i.e., the parallel and the cross wire techniques.

[1] Physikalisch-Technische Bundesanstalt, Bundesallee 100, D-38116 Braunschweig, Germany.
[2] To whom correspondence should be addressed. E-mail: Ulf.Hammerschmidt@PTB.DE.

In the standard configuration, a thin metal wire, clamped between two brick-shaped sample halves, simultaneously acts as a resistive heat source and a thermometer. The surroundings serve as a heat sink at constant operating temperature. The temperature-dependent voltage drop across the wire provides a measure of the thermal transport properties mentioned above.

In the last few years, another transient technique appeared that is closely related to the standard THW technique, the transient hot strip (THS) method. Here, instead of the wire, a thin metal foil is used as the active thermal transport property sensor. Advantages of this slight modification arise mainly from two factors: (1) due to the strip geometry, a THS setup is easier to arrange than a THW setup; and (2) due to its greater surface and smaller thickness ($v = 0.01$ mm), the density of heat flow of the strip and its thermal contact resistance to the sample may be significantly lower than for a wire. However, as has been shown in Ref. 6, the expanded ISO standard uncertainty for a coverage factor of $k = 2$ of a typical THS setup is 5% for the thermal conductivity and 22% for the thermal diffusivity as assessed against the standard reference CRM 039 (Pyrex). The THW uncertainty of the thermal conductivity, as found in the literature, is claimed to be better than 5% (cf., e.g., Ref. 1).

The objective of this paper is to estimate the ISO uncertainty [7] of the standard THW setup under almost the same conditions as for the THS instrument. In accordance with Ref. 6, we analyze three types of major errors caused by the model, the evaluation procedure, and the measuring instruments. Within the scope of this investigation, the sensitivity of λ and a to errors of the measurement inputs is quantified. The uncertainty estimated for the thermal conductivity of CRM 039 is confirmed experimentally.

2. THEORY

A very long metal wire of radius $r \to 0$ is entirely embedded in an unbounded homogeneous and isotropic dielectric solid, initially at the temperature $T(r, t = 0) = T_0$. When a constant electric current I is passed through the wire, the latter simultaneously serves as a continuous heat source of rate $\Phi = UI$ and as a resistance thermometer of output voltage $U(T(t))$. This transient signal provides a measure of the thermal conductivity λ and diffusivity a of the sample. It is specified to a good approximation by the line source solution of the conduction equation:

$$\Delta U(T(t)) = U(T(t)) - U_0 = \frac{\alpha U_0^2 I}{4\pi L\lambda} f_{\mathrm{W}}(\tau) = c(\lambda)\, f_{\mathrm{W}}(\tau) \qquad (1)$$

Here

$$f_{\mathrm{W}}(\tau) = -\mathrm{Ei}(-\tau^{-2}) \tag{2}$$

and

$$\tau = \frac{\sqrt{4at}}{r} \tag{3}$$

U_0 denotes the voltage drop at $t = 0$ and α is the temperature coefficient of the electrical resistance of the wire of length L.

In practice, a THW signal $U(t)$ is monitored pointwise as the time series of N ordered pairs $U(t_i) = U(t_0), U(t_1), U(t_2), \ldots, U(t_N)$. By evaluation of the amplitude $c(\lambda)$ and shape $f_{\mathrm{W}}(\tau(a))$ of this signal, the thermal conductivity λ and the thermal diffusivity a of a finite sample can basically be determined. However, since the model is derived for a one-dimensional continuous heat source and an infinite sample, the nonvanishing heat capacity of the real wire and the exposed outer surface of the real sample are not encountered. Equation (1) therefore is practically valid only for a limited interval of time, $[0 < t_{\min}, t_{\max}]$, during which the thermal influence of the wire can be confined to the sample itself.

As can be seen from the literature (cf., e.g., Ref. 1), the nonlinear and implicit expression, Eq. (1), is linearized with respect to $\ln \tau$ by expanding $f_{\mathrm{W}}(\tau)$ in a McLaurin series and retaining the first two terms only. For values of $1/\tau \ll 1$, the expression,

$$U(t) - U_0 \approx \frac{\alpha U_0^2 I}{4\pi L\lambda}\left(\ln t + \ln \frac{4a}{r^2} - \gamma\right) = cF_{\mathrm{W}}(t) = ct' + d \tag{4}$$

sufficiently approximates the THW voltage signal $U(t)$ during the time segment $[t_{\min}, t_{\max}]$. In Eq. (4), $\gamma = 0.5772\ldots$ is Euler's constant and t' stands for $\ln t$. The constants $c = \alpha U_0^2 I/(4\pi L\lambda)$ and $d = c(-\gamma + \ln 4a/r^2)$ are the slope and intercept, respectively, of the line segment. Both unknown parameters can be determined from a monitored THW signal, $\Delta U_i(t)$, according to

$$c = \frac{\sum t_i' \sum \Delta U_i - N \sum t_i' \, \Delta U_i}{(\sum t_i')^2 - N \sum t_i'^2} \tag{5}$$

and

$$d = \frac{1}{N}\left(\sum \Delta U_i - c \sum t_i'\right) \tag{6}$$

Table I. Formal Correspondence Between the THW Mathematical Model and the Linear and Nonlinear THS Models (D: Strip Width)

Method	Slope/amplitude	Intercept/shape
THW	$c = \alpha U_0^2 I/4\pi L\lambda$	$d = c(-\gamma + \ln 4a/r^2)$
THS		
Linear	$m = \alpha U_0^2 I/4\pi L\lambda$	$n = m(3 - \gamma + \ln 4a/D^2)$
Nonlinear	$k(\lambda) = \alpha U_0^2 I/2\sqrt{\pi}\, L\lambda$	$f(\tau(a)) = \tau\,\mathrm{erf}(\tau^{-1}) - \frac{\tau^2}{\sqrt{4\pi}}[1 - \exp(-\tau^{-2})] - \frac{1}{\sqrt{4\pi}}\mathrm{Ei}(-\tau^{-2})$

respectively. The measurands finally follow from

$$\lambda = \frac{\alpha U_0^2 I}{4\pi L c} \tag{7}$$

and

$$a = \frac{r^2}{4}\exp\left(\frac{d}{c} + \gamma\right) \tag{8}$$

Formal correspondences between the THW mathematical model, on the one hand, and the nonlinear and the linear THS [6] models, respectively, on the other hand, are listed in Table I.

Any observed THW signal, $U(t_i)$, deviates from an ideal signal, $U^*(t)$, by a certain time-dependent amount, namely, $\Delta U(t_i)$. $\Delta U(t_i)$ is due to different error sources that can be divided into three characteristic groups: first, errors due to the instrumentation, $\Delta\delta U^{\mathrm{J}}$; second, random evaluation errors, δU^{E}; third, specific model errors, δU^{M}. They all depend on time in their characteristic way.

$$U(t) = U^*(t) + \delta U(t) = U^*(t) + \delta U^{\mathrm{M}}(t) + \delta U^{\mathrm{E}}(t) + \delta U^{\mathrm{J}}(t) \tag{9}$$

2.1. Ideal Model Errors

A THW setup can be analytically treated only for the ideal physical model as outlined above. This thermally closed system has a simple balance: the electric power, $P = UI$, fed to the line source, is completely and instantly liberated to the sink (sample), where it is continuously stored.

In contrast to the ideal model, the experimental setup has to be considered an open system because of its inner and outer thermal leakages. At the inner boundary, first, a certain fraction $\Phi_{11}(\tau)$ of the input power $\Phi_0 = P$ flows "into" the wire, where it is stored due to the wire's nonzero heat capacity. Second, if the sample is not opaque, the fraction $\Phi_{12}(\tau)$ of the output power of the wire can be transferred by radiation through the sample. At the outer boundary, due to its finite radius and length, the cylindrical sample liberates an additional fraction, $\Phi_{21}(\tau)$, to the lateral surfaces and a fraction $\Phi_{22}(\tau) = 2\Phi_{\text{fin}}$ to both bases (cf. Fig. 3). All four interactive transport mechanisms introduce characteristic model errors, namely, $\delta U^{\text{W}}(\tau_i)$, $\delta U^{\text{S}}(\tau_i)$, $\delta U^{\text{R}}(\tau_i)$, and $\delta U^{\text{L}}(\tau_i)$. They depend on time τ, however, each in a different way. The error $\delta U^{\text{W}}(\tau_i)$ becomes effective for times $\tau < 1$ only, whereas $\delta U^{\text{R}}(\tau_i)$, $\delta U^{\text{S}}(\tau_i)$, and $\delta U^{\text{L}}(\tau_i)$ give rise to non-linear deviations for long times. In contrast to the first error, the latter can be easily identified as a departure from linearity of the signal plot U_i vs ln t [Eq. (4)].

2.1.1. *Inner Boundary*

2.1.1.1. Nonvanishing Heat Capacity of the Wire. A wire of volume $V = \pi r^2 L$, density ρ^{W}, and specific heat capacity c_{P}^{W} can store heat at a net rate $\Phi_{11} = -V(\rho^{\text{W}} c_{\text{P}}^{\text{W}} - \rho c_{\text{P}})\,\mathrm{d}T^{\text{W}}/\mathrm{d}t$. Here, ρ and c_{P} are the sample's density and specific heat, respectively. Thus, there is a stray heat flow Φ_{11} "into" the wire when this is self-heated by the constant electric power Φ_0 [8]. While Φ_{11} is stored, the mean temperature of the wire T^{W} rises accordingly. The associated model error δU^{W} can be expressed by the working equation, Eq. (10),

$$\delta U^{\text{W}} = \frac{\Phi_{11}(\tau_i)}{\Phi_0}\, c f_{\text{W}}(\tau_i) \tag{10}$$

where

$$\frac{\mathrm{d}T^{\text{W}}}{\mathrm{d}t} = \frac{c}{\alpha U_0(t)} \exp\left(-\frac{r^2}{4at}\right)$$

and

$$\delta U^{\text{W}} = \frac{r^2(\rho^{\text{W}} c_{\text{P}}^{\text{W}} - \rho c_{\text{P}})}{4\lambda} \frac{1}{t_i} \exp\left(-\frac{1}{\tau_i^2}\right) c \left[-\text{Ei}\left(-\frac{1}{\tau_i^2}\right)\right] \tag{11}$$

Within the limit $t \to 0$, the right-hand side of Eq. (10) becomes $|\Phi_{11}/\Phi_0| \to 1$. When the experiment starts, the total input power is consumed by the wire. But just 1 s later, the ratio of heat flows rapidly drops to typically $|\Phi_{11}/\Phi_0| \approx 1\%$ because of the low heat capacity of the wire.

2.1.1.2. Radiation Loss. The cylindrical sample is enclosed in a cell whose length is much greater than its diameter $2R$. The wire of radius $r \ll R$ and the inner surfaces of the cell are diffusively gray radiators; the sample is transparent. The exchange of energy between the wire and the cell by radiation heat transfer is given by

$$\Phi_{12} = \frac{[2\pi r L\sigma(T^4 - T_0^4)]}{\left[\dfrac{1}{\varepsilon^{\mathrm{W}}} + \dfrac{r}{R}\left(\dfrac{1}{\varepsilon^{\mathrm{C}}} - 1\right)\right]} \tag{12}$$

Here, ε^{W} and ε^{C} are the total emissivities of the wire and the cell, respectively; σ is the Stefan–Boltzmann constant [9]. Taking into account that $\varepsilon^{\mathrm{C}} > \varepsilon^{\mathrm{W}}$ and $T - T_0 \ll T_0$, Eq. (12) can be simplified to

$$\Phi_{12} \approx 8\pi r\varepsilon^{\mathrm{W}} L\sigma T_0^3 (T - T_0) \tag{13}$$

Now the model error induced by radiation heat transfer can be written

$$\delta U^{\mathrm{S}} = \frac{\Phi_{12}}{\Phi_0} cf_{\mathrm{W}}(\tau_i) \tag{14}$$

Expressed in nondimensional units, the resulting equation is

$$\frac{\delta U^{\mathrm{S}}}{\Delta U} = \frac{\Phi_{12}(\tau_i)}{\Phi_0} = \frac{2r\varepsilon^{\mathrm{W}}\sigma T_0^3}{\lambda}(2 \ln \tau_i - \gamma) \tag{15}$$

Thus, for a given working temperature T_0, the error due to the wire's radiative heat transfer increases in time as $\ln \tau$. The constant of proportionality is $\varepsilon^{\mathrm{W}}/\lambda$, the ratio of the wire's total emissivity to the thermal conductivity of the sample.

2.1.2. Outer Boundary

2.1.2.1. Finite Length of the Sample. The ideal model underlying the THW technique is that of an endless line source (wire) embedded in an unbounded sample. Here, the heat, emitted by the source, flows radially through the sample resulting in concentric isotherms. In practice, the cylindrical sample has not only a finite radius but also a finite length. At both cylinder bases, there are stray heat flows out of the sample so that the mean temperature of the wire does not increase to the values predicted by theory. The radial–axial transient heat flow problem has been analyzed for different boundary conditions and borderline cases in, e.g., Refs. 10 and 11. As expected, all given solutions indicate that the error due to axial heat flow, $\delta U^{\mathrm{L}}(t_i)$, depends on the ratio $L^* = L/(2r)$. The error increases with time and approaches particularly large values for a sample whose heat capacity is low compared to that of the wire. A general solution of the problem under discussion is presented in Ref. 12 for isothermal boundary conditions in radial and axial directions. The mean wire temperature can be written

$$T^*(\tau) = \frac{P}{L\lambda} G^*(L^*, \omega, \beta, \tau) \tag{16}$$

with

$$G^* = \frac{16}{\pi^4} \sum_{k=0}^{\infty} \frac{1}{(2k+1)^2} \times \int_0^\infty \frac{1 - \exp\{-[((2k+1)\pi/L^*)^2 + u^2](\tau^2/4)\}}{[((2k+1)\pi/L^*)]^2 + u^2} uf(u)\, du \tag{17}$$

$$f(u) = \frac{[Y_0(u)\,\Phi(u) - J_0\,\Psi(u)]}{[\Phi^2(u) + \Psi^2(u)]} \tag{18}$$

$$\Phi(u) = 2\left[uJ_1(u) + \left[\left(\frac{1}{\beta} - \frac{1}{\omega}\right)\left(\frac{\pi(2k+1)r}{L}\right)^2 - \frac{u^2}{\omega}\right] J_0(u)\right] \tag{19}$$

$$\Psi(u) = 2\left[uY_1(u) + \left[\left(\frac{1}{\beta} - \frac{1}{\omega}\right)\left(\frac{\pi(2k+1)r}{L}\right)^2 - \frac{u^2}{\omega}\right] Y_0(u)\right] \tag{20}$$

Here, $J_0(\cdots)$ and $J_1(\cdots)$ are the first-kind and $Y_0(\cdots)$ and $Y_1(\cdots)$ are the second-kind Bessel functions of zero order and first order, respectively; $\omega = \rho c_{\mathrm{P}}/(\rho^{\mathrm{W}} c_{\mathrm{P}}^{\mathrm{W}})$ and $\beta = \lambda/\lambda^{\mathrm{W}}$. As mentioned above, the superscript "W" indicates properties related to the wire. The voltage error associated with the finite wire length is specified by

$$\frac{\delta U^{\mathrm{L}}}{U} = 1 - 4\pi \frac{G^*(L^*, \omega, \beta, \tau_i)}{f_{\mathrm{W}}(\tau_i)} \tag{21}$$

To keep axial heat loss error within a few percent, there are three conditions [12] that have to be fulfilled at isothermal boundaries: $\sqrt{\omega}\, L^* > 500$, $\sqrt{\beta}\, L^* > 500$, and $100 < \omega t^* < 1000$. These requirements are easily met for materials having higher thermal conductivities and heat capacities than gases, i.e., for liquids and solids. Especially for solids in gas-filled vessels, the errors due to finite wire length are in fact significantly lower than predicted by Eq. (21) because the boundary conditions at the bases of the sample are adiabatic rather than isothermal.

2.1.2.2. Finite Radius of the Sample. In order to quantify the error $\delta U^{\mathrm{R}}(\tau_i)$ caused by the density of heat flowing outward, $\Phi'_{21}(R_0, \tau)/A$, at the exposed lateral surface $A(R = R_0)$ of a finite sample, its actual outer boundary conditions must first be specified: for simplicity's sake, a cylindrical sample of finite radius $R = R_0$ is considered a subsystem cut out of the homogeneous and isotropic infinite sample. According to the basic theory, the subsystem's interfacial area A is crossed by the heat flux $\Phi'_{\mathrm{P}}(R_0, \tau)/A$. It follows that the error $\delta U(\tau_i)$ varies directly with the difference of both heat flows, Φ'_{21} and Φ'_{P}:

$$\Phi_{21} = \Phi'_{21} - \Phi'_{\mathrm{P}} \tag{22}$$

Obviously, δU^{R} gets closer to zero as the stray heat flux Φ'_{21}/A approaches the value of the equivalent virtual heat flux within the infinite sample. This is the same situation as with the THS method. As has been discussed at some length for this technique in Ref. 6, the thermal situation at the surface of a finite sample can be interpreted as a nonlinear boundary condition of the second kind:

$$\lambda^{\mathrm{C}} \left.\frac{\partial T}{\partial n}\right|_{R_0} = \frac{\Phi'_{21}(R_0, t)}{A} \tag{23}$$

Here, λ^{C} denotes the thermal conductivity of a sample holder and $\partial T/\partial n$ is the derivative along the outward normal to the surface A. While $\Phi'_{\mathrm{P}}(R_0, t)/A$ can be calculated from the ideal model, $\Phi'_{21}(t)$ cannot be exactly defined for a given outer boundary condition. However, two special cases, in which (1) $\lambda^{\mathrm{C}} \gg \lambda$ or (2) $\lambda^{\mathrm{C}} \ll \lambda$, lead to analytical solutions [13]. For $\lambda^{\mathrm{C}} \gg \lambda$, the finite sample surface may be considered quasi-isothermal (homogeneous boundary condition of the first kind). Then its temperature excursion, $T'(R_0, t)$, is governed by the equation

$$T'(t) = T_0 + \frac{\Phi}{4\pi L\lambda} \ln\left(\frac{R_0}{r}\right)^2 - 4 \sum_{n=1}^{\infty} \frac{J_0(\mu_n r/R_0)}{\mu_n^2 J_1^2(\mu_n)} \times \left[\frac{\Phi}{4\pi L\lambda} + \frac{1}{2} T_0 \mu_n J_1(\mu_n)\right] \exp\left(-\frac{\mu_n^2 a t}{R_0^2}\right) \tag{24}$$

where, again, $J_0(\cdots)$ and $J_1(\cdots)$ are the first-kind Bessel functions of zero order and first order, respectively. The second case of particular interest is the quasi-adiabatic surface where $\lambda^{C} \ll \lambda$ (boundary condition of the fourth kind):

$$T'(t) = T_0 + \frac{\Phi}{4\pi L\lambda}\left[\frac{4at}{R_0^2} + \frac{r^2}{R_0^2} + 2\ln\frac{R_0}{r} - \frac{3}{2} - 4\sum_{n=1}^{\infty}\frac{J_0(\mu_n r/R_0)}{\mu_n^2 J_0^2(\mu_n)}\exp\left(-\frac{\mu_n^2 at}{R_0^2}\right)\right] \tag{25}$$

The eigenvalues of Eqs. (24) and (25) are given by

$$J_0(\mu) = 0 \qquad \text{and} \qquad J_1(\mu) = 0 \tag{26}$$

respectively.

Some numerical results for $R_0 = 10r$ and $k = U_0 I/(4\pi L\lambda) = 1$ K are shown in Fig. 1 vs the nondimensional time $\tau(R_0)$, which is related here to the characteristic length $R = R_0$. As shown in this figure, any THW signal can be observed only within the area between the limiting curves denoted "adiabatic" and "isothermal." Figure 2 represents departures in the temperature excursions of an adiabatically and an isothermally bounded finite sample from those of the ideal sample. Obviously, a THW/THS experiment

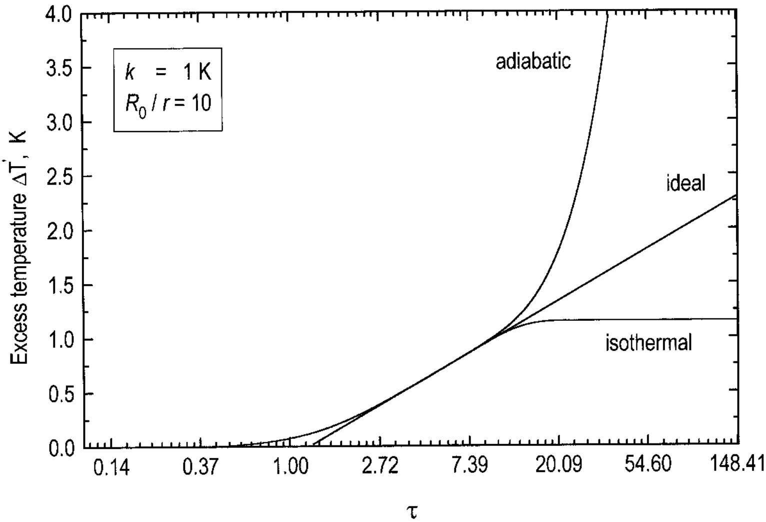

Fig. 1. Linear heat source excess temperature vs nondimensional time for three boundary conditions (cf. text).

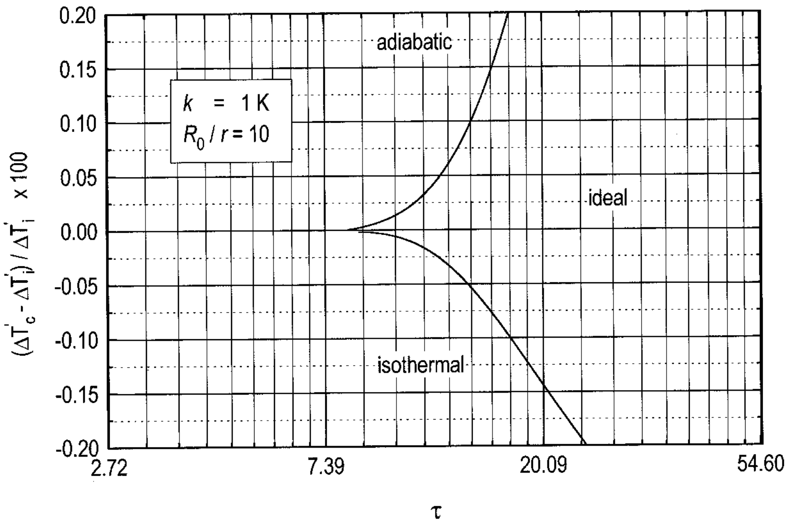

Fig. 2. Difference between an ideal and a real curve with isothermal or adiabatic boundary conditions vs nondimensional time (cf. Fig. 1).

can be run under near-adiabatic[3] or under near-isothermal boundary conditions without any major change in quality within a limited period of time.

To show both above-mentioned outer boundary conditions during one experimental run on a reference specimen, we used a massive metal sample holder ($\lambda^{CM} \gg \lambda$) which was thermally coated on its outer surfaces with an insulating material ($\lambda^{CI} \ll \lambda$). As shown in the signal plot (Fig. 3), after 2 s, the excess temperature of the wire first inclines quasi-linearly. This effect can be observed as long as the thermal wave travels through the sample exclusively. The quasi-ideal segment is denoted "L1." It ends when, after some time, the sample holder is reached. Due to the near-isothermal conditions, the temperature of the wire rises only slightly during segment "L2." As time goes on, the wave front leaves the holder for the coating. Here, near-adiabatic conditions are realized; the temperature then increases rapidly.

To calculate the error $\delta U^{R}(t_i)$ due to its finite size, the cylindrical sample is considered here to be encapsulated in a metal sample holder of thermal conductivity $\lambda^{CM} \gg \lambda$. The holder itself is kept at a constant temperature $T = T_0$, e.g., in a thermostated bath. Assuming that the temperatures for an unbounded and a finite sample in pairs differ by the same

[3] The prefix "near" means "as close as practically possible."

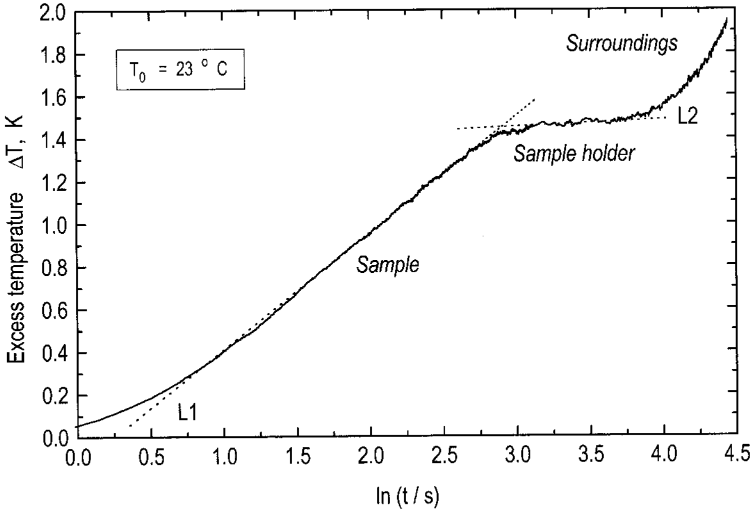

Fig. 3. THW excess temperature vs ln t monitored for a Pyrex *sample* encapsulated in a massive metal *sample holder* surrounded by a thermally insulating board (*surroundings*) under room conditions. (cf. Fig. 1, curves "isothermal" and "adiabatic").

value when measured at the wire, $R=r$, and at $R=R_0$, the following approximation for the finite sample can be derived:

$$f'_{\mathrm{W}}((\tau) \approx -\mathrm{Ei}\left(-\frac{r^2}{4at}\right)+\mathrm{Ei}\left(-\frac{R_0^2}{4at}\right) \tag{27}$$

The differences among the closed form approximation, Eq. (27), the exact solution, Eq. (25), and the linearized case, Eq. (2), can be seen in Fig. 4.

Now the error $\delta U^{\mathrm{R}}(t_i)$ in the voltage drop of the wire can easily be formulated in terms of Eq. (27):

$$\delta U^{\mathrm{R}}(t_i)=\alpha U_0[T'(0, t_i)-T(0, t_i)]=\alpha\frac{U_0^2 I}{4\pi L\lambda}\,\mathrm{Ei}\left(-\frac{R_0^2}{4at_i}\right) \tag{28}$$

and

$$\frac{\delta U^{\mathrm{R}}(t_i)}{U}\approx\frac{\delta U^{\mathrm{R}}(t_i)}{U_0}=\alpha\frac{\Phi}{4\pi\lambda L}\,\mathrm{Ei}\left(-\frac{R_0^2}{4at_i}\right) \tag{29}$$

The exponential integral $-\mathrm{Ei}(-R_0^2/4at_i)$ does not have a significant effect on the error δU^{R} for arguments $R_0^2/4at_i<0.5$. This is the case for a maximum excess temperature of surface A of about 0.1 K. From $R_0^2/4at_t\approx 0.5$

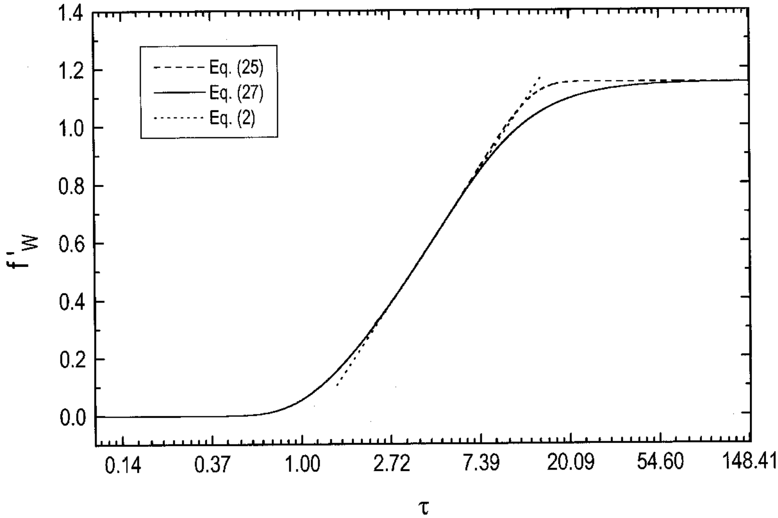

Fig. 4. Exact [Eq. (25)] and approximated [Eq. (27)] THW shape function vs. nondimensional time for an isothermally bounded sample. Equation (2) represents the ideal sample (cf. text).

the error begins to increase rapidly with time. An experiment should therefore be stopped at $t_{\max} \leqslant R_0^2/2a$ (cf. Ref. 8).

2.2. Linear Model Error

Due to the asymptotic form of the linearization of Eq. (1), there is a certain deviation from this ideal model function. In Fig. 5, the relative truncation error of $F_W(\tau)$ is plotted vs τ as the percentage deviation from its origin, $f_W(\tau)$. For comparison, the diagram also shows the related linear procedure error of the THS method, denoted as F_2 [6]. Surprisingly, the departure of the linearized THS function F_2 from the original function is smaller than that of the expression analyzed here.

From the data set $[F_W(\tau_i) - f(\tau_i)]/f(\tau_i)$ calculated pointwise, as plotted in Fig. 5, the linear model error in λ and a cannot be derived directly because it does not depend only on $\tau_{\min}(t_{\min})$, but also on the other end point, $\tau_{\max}(t_{\max})$, of the linear segment of the signal $[\tau_{\min}, \tau_{\max}]$. Since this error is introduced by the truncation of the Ei series, it can be expressed to a good approximation by the remainder R_2, which is given by the third term of the expansion:

$$-\mathrm{Ei}\left(-\frac{1}{\tau^2}\right) = -\gamma - \ln\left(\frac{1}{\tau^2}\right) + \left(\frac{1}{\tau^2} - \frac{1}{4\tau^4} - \dots\right) \approx -\gamma + \ln \tau^2 + \frac{1}{\tau^2} \tag{30}$$

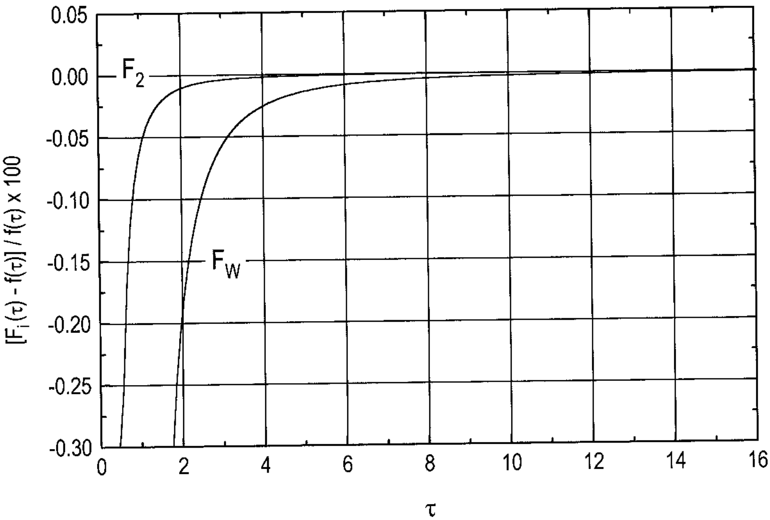

Fig. 5. Deviation of quasi-linear functions F_W and F_2 from the related THW/THS shape functions $f_W(\tau)$ and $f(\tau)$, respectively, vs nondimensional time τ as a percentage (cf. text).

$R_2 = c(1/\tau^2) = cr^2/4at$ is now analyzed as the first-order deviation of voltage $\delta U^L(t_i)$ due to linearization. The approximate relative error now reads $[\tau^2(\ln \tau^2 - \gamma)]^{-1}$. Expressed in terms of the time-dependent error δU^L, the following is obtained for each pair of experimental data $U(t_i)$:

$$\delta U^L = \frac{cr^2}{4at_i} = \frac{c}{\exp((d/c)+\gamma)\exp(t_i')} \tag{31}$$

For the linear segment of an observed THW signal, the induced deviations from both measured quantities, c and d, are given by

$$u_{\text{lin}}(c) = \frac{c}{\exp((d/c)+\gamma)} \frac{\sum t_i' \sum \exp(-t_i') - N \sum t_i' \exp(-t_i')}{(\sum t_i')^2 - N \sum t_i'^2} \tag{32}$$

and

$$u_{\text{lin}}(d) = \frac{1}{N}\left[\frac{c}{\exp((d/c)+\gamma)} \sum \exp(-t_i') - m \sum t_i'\right] \tag{33}$$

A numerical evaluation of Eqs. (32) and (33) with respect to the measurands λ and a yields the plots in Figs. 6 and 7. Separately for both

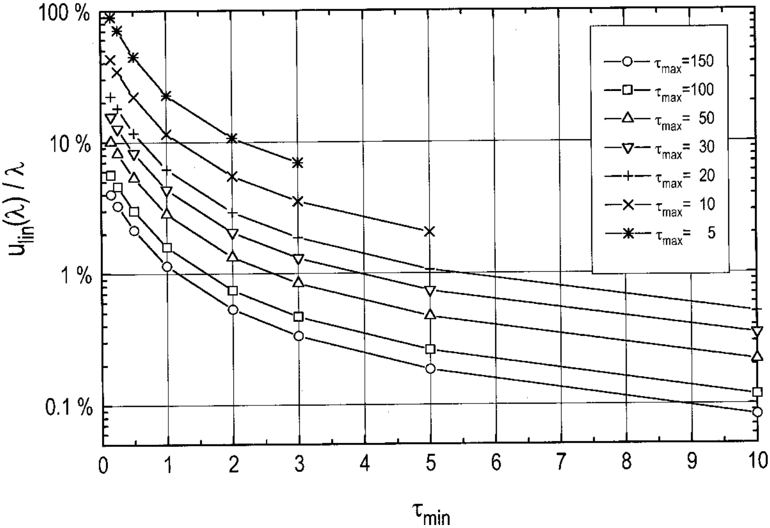

Fig. 6. Model error of measured thermal conductivity λ caused by linearization of Eq. (1). The error has been plotted in terms of different upper end points τ_{max} of any linear interval.

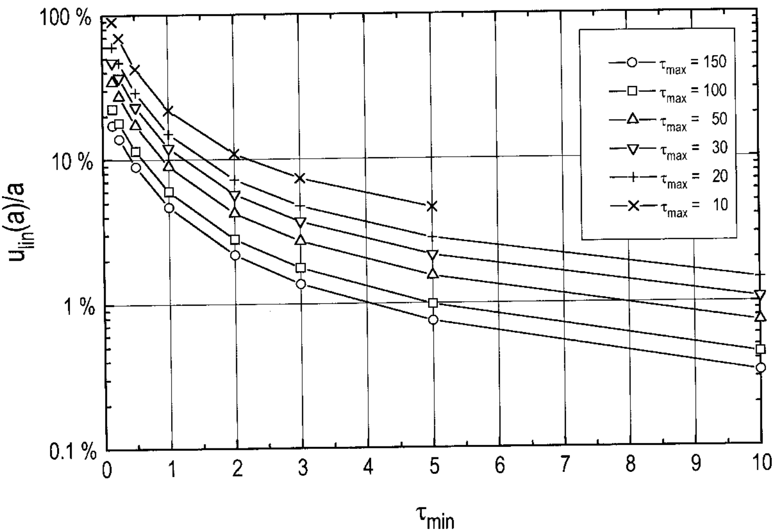

Fig. 7. Model error of measured thermal diffusivity a caused by linearization of Eq. (1). The error has been plotted in terms of different upper end points τ_{max} of any linear interval.

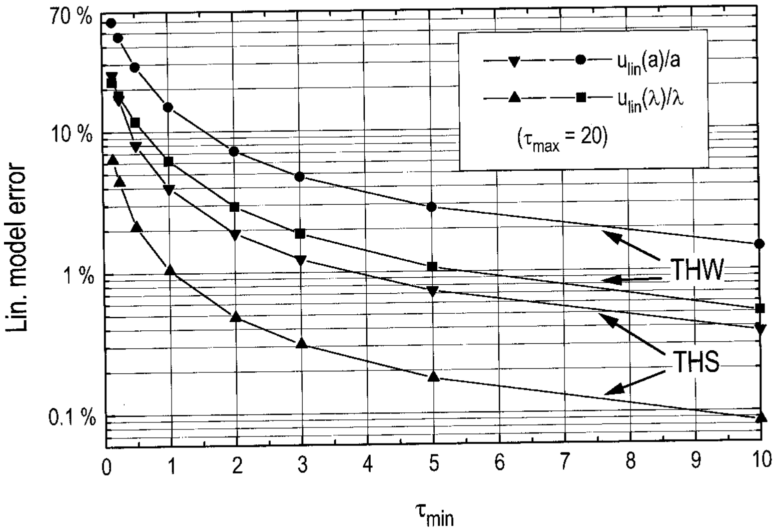

Fig. 8. Percentage linear model error of measured thermal conductivity λ and thermal diffusivity a for an upper end point $\tau_{max} = 20$ for the THW and THS [6] methods. The error has been plotted vs the lower end point of any linear time interval (cf. text).

measurands, they show the effect which a variation of the upper end point τ_{max} between 5 and 150 exerts on the related model error in terms of the lower end point τ_{min}. For more convenient comparison, numerical values of $u_{lin}(\lambda)/\lambda$ and $u_{lin}(a)/a$ vs τ_{min} are plotted in Fig. 8 for a fixed value of $\tau_{max} = 20$. As shown more rigorously later [Eqs. (37) and (38)], the model error linked with thermal diffusivity is larger than that linked with thermal conductivity. The chart also shows the related values for the THS method.

2.3. Evaluation Error

An observed THW signal is always subject to random errors causing deviations from the signal predicted by the underlying linear model. The model parameters c and d can therefore be estimated only to a restricted degree of confidence that is expressed here in terms of the confidence intervals $u_A(c)$ and $u_A(d)$. These intervals are associated with a characteristic confidence level P. The confidence intervals of any model parameters b_m are generally given by

$$u_A(b_m) = F(P, j)\,\frac{\chi^2}{N-j}\,\alpha^*_{mm} \tag{34}$$

Here, $F(P, j)$ is a function of probability depending on j as the degree of freedom and on P as the confidence level. χ^2 denotes the sum of square deviations of N data points and α^*_{mm} is an element of the inverted Hessian [6]. In the case of a simple linear regression model ($j=2$) and a percentage confidence level of $P=68.3\,\%$,[4] the probability function provides $F(0.683,2)=2.3$, and both diagonal elements of the matrix α^* are

$$\alpha^*_{11}=\frac{\sum t_i'^2}{N\sum t_i'^2-(\sum t_i')^2} \tag{35}$$

$$\alpha^*_{22}=\frac{N}{N\sum t_i'^2-(\sum t_i')^2} \tag{36}$$

When Eqs. (35) and (36), respectively, are inserted into Eq. (34), the confidence intervals for parameters c and d, referred to as standard uncertainties of type A, are written as follows:

$$u_{\mathrm{A}}(c)=\sqrt{\frac{2.3\chi^2}{N-2}\cdot\frac{N}{N\sum t_i'^2-(\sum t_i')^2}} \tag{37}$$

$$u_{\mathrm{A}}(d)=\sqrt{\frac{2.3\chi^2}{N-2}\cdot\frac{\sum t_i'^2}{N\sum t_i'^2-(\sum t_i')^2}} \tag{38}$$

2.4. Measurement Errors

In close analogy with Ref. 6, we take the four most significant measurement errors, δU^{J}, into account. Three of these stem from the electrical part of the setup. First, to simplify the experiment, the wire is heated not by constant power but by constant current. Since the resistance of the wire, $R(T)$, depends on the temperature, this mode results in a continuous growth of the heat flow Φ_0 as given by $\Phi_0=P=R(T)\,I^2$. Second, the instability of the current source, δI, causes a departure of the THW voltage signal, namely, $U(t_i)\,\delta I/I$. Due to the limited accuracy and nonvanishing integration time of the voltmeter, the measurement is affected by an error δU^{V}. Third, even in well thermostated setups, an additional error of the measured voltage arises from a temperature drift in the sample. It follows that

$$\delta U^{\mathrm{J}}=\delta U^{\mathrm{P}}+\delta U^{\mathrm{V}}+\delta U^{\mathrm{I}}+\delta U^{\mathrm{T}} \tag{39}$$

[4] A 68.3% confidence interval is chosen for now. In Section 3, the evaluation error is added to all the other errors discussed here and the sum is then multiplied by a coverage factor of $k=2$. This leads to the usual confidence level of 95%.

Here, the superscripts denote the following potential error sources.

P: Constant current mode
V: Nonideal voltmeter
I: Instability of current source
T: Temperature drift

2.4.1. Constant-Current Mode

The electrical resistance $R(T)$ of the Joule-heated wire increases continuously in terms of its temperature T. When a constant current I is fed to the wire, it generates a heat flow that is not constant but varies at a rate $P = UI = R(T)\,I^2$. This effect causes an error δU^{P} of the measured voltage signal.

To determine the influence of the temperature-dependent generation rate within Eq. (1), the constant power $U_0 I$ is replaced by $U(t)\,I_0$. After some rearrangements, the working equation reads as follows:

$$U(t) = \frac{U_0}{1 - (c/U_0)\, f_{\mathrm{W}}(\tau)} \tag{40}$$

A Taylor series expansion of $U(t)$ about $cf_{\mathrm{W}}(\tau)/U_0$ is used to determine the error since $cf_{\mathrm{W}}(\tau)/U_0 \ll 1$:

$$U(t) = U_0 + cf_{\mathrm{W}}(\tau) + \frac{c^2}{U_0} f_{\mathrm{W}}{}^2(\tau) + \cdots \tag{41}$$

The difference between Eq. (1) and Eq. (41) is represented by the third term on the right-hand side of the latter expression because higher-order terms may be neglected in view of the above-mentioned inequality. Thus,

$$\delta U^{\mathrm{P}} = \frac{c^2}{U_0}\, \mathrm{Ei}^2\left(\frac{1}{\tau^2}\right) \tag{42}$$

In terms of the nondimensional time τ, three cases can be considered.

1. $$\tau \ll 1 \Rightarrow \delta U^{\mathrm{P}} = \frac{c^2}{U_0}\, \tau^2 \tag{43}$$

2. $$\tau = 1 \Rightarrow \delta U^{\mathrm{P}} = 0.53\, \frac{c^2}{U_0} \tag{44}$$

3. $$\tau \gg 1 \Rightarrow \delta U^{\mathrm{P}} = \frac{c^2}{\pi U_0}\, (1.21 + \ln \tau)^2 \tag{45}$$

During a normal THW run all three cases occur successively.

2.4.2. Voltage Measurement

Errors of the measured voltage, δU^{V}, of the monitored signal $U(t_i)$ are in most cases caused by three effects: the finite precision of the voltmeter $u(U)$, its nonvanishing integration time δt while the signal rises as $k(\partial f(\tau_i)/\partial t)$, and the current source uncertainty $u(I)$. Both instrument uncertainties, $u(U)$ and $u(I)$, depend on time. Their systematic components are covered by Eq. (1). Their random components cause an increase in the χ^2 deviations of the observed signal from the fitted one. As A-type uncertainties, they have already been accounted for in Section 2.3. Thus, the residual time-dependent voltage error is introduced by the integration time of the voltmeter and the transient signal rise:

$$\delta U^{\mathrm{V}} = -\delta t\, c \frac{\partial}{\partial t}\left[\mathrm{Ei}\left(-\frac{1}{\tau^2}\right)\right] = \frac{\delta t}{t}\, c \exp\left(-\frac{r^2}{4at}\right) \tag{46}$$

2.4.3. Ambient Temperature Variation

Any variation of the temperature of the sample environment, $\mathrm{d}T_{\mathrm{D}}/\mathrm{d}t$, gives rise to a departure of the measured voltage signal of

$$\delta U^{\mathrm{T}} = \alpha U_0 \frac{\mathrm{d}T_{\mathrm{D}}}{\mathrm{d}t}\, t_i \tag{47}$$

3. STANDARD UNCERTAINTY

According to Ref. 7 the combined standard uncertainty $u_{\mathrm{c}}(y)$ of the quantity y is the positive square root of the combined variance $u_{\mathrm{c}}^2(y)$ obtained from

$$u_{\mathrm{c}}^2(y) = \sum_{i=1}^{N} \left(\frac{\partial y(\vec{x})}{\partial x_i}\right)^2 u^2(x_i) \tag{48}$$

where $u^2(x_i)$ are the variances of the input quantities x_i. The partial derivatives of y with respect to x_i are referred to as sensitivity coefficients.

For the THW method, all sensitivity coefficients can readily be analytically calculated because of the explicit character of the model equation, Eq. (4). From this expression, working equations are derived for both measurands [Eqs. (7) and (8)]. The combined variances for λ and a are obtained from the time-independent standard uncertainties of the input quantities and the linear model errors:

$$\left(\frac{u_c(\lambda)}{\lambda}\right)^2 = \left(\frac{u(\alpha)}{\alpha}\right)^2 + \left(\frac{u(I)}{I}\right)^2 + \left(\frac{u(L)}{L}\right)^2 + \left(\frac{u(U_0)}{U_0}\right)^2 + \left(\frac{u(c)}{c}\right)^2 + \left(\frac{\delta\lambda}{\lambda}\right)^2 \tag{49}$$

$$\left(\frac{u_c(a)}{a}\right)^2 = \left(2\,\frac{u(r)}{r}\right)^2 + \left(\frac{d}{c}\frac{u(d)}{d}\right)^2 + \left(\frac{d}{c}\frac{u(c)}{c}\right)^2 + \left(\frac{\delta a}{a}\right)^2 \tag{50}$$

The model errors are taken into account in each case by the last term on the right-hand sides of the two equations. The variances of input quantities α, I, L, U_0, and r can readily be calculated, whereas those of parameters c and d consist of two subcomponents of type A and type B according to Ref. 7:

$$\left(\frac{u(c)}{c}\right)^2 = \left(\frac{u_A(c)}{c}\right)^2 + \left(\frac{u_B(c)}{c}\right)^2 \tag{51}$$

$$\left(\frac{u(d)}{d}\right)^2 = \left(\frac{u_A(d)}{d}\right)^2 + \left(\frac{u_B(d)}{d}\right)^2 \tag{52}$$

The A-type terms are already defined by Eqs. (37) and (38). They vary directly as the root mean square value of χ, which itself depends on the current source noise in particular. Since the current noise is randomly distributed, both A-type terms do not depend on time. The B-type terms, defined by Eq. (9), allow for systematic voltage deviations. These seven time-dependent errors are caused by the nonzero heat capacity of the wire, thermal radiation, outer boundary conditions (axial and radial heat losses), nonconstant power supply, finite integration time of the voltmeter, and temperature drift of the sample surroundings. In principle, if systematic errors and their causes are known, they can be compensated by corrections. However, each of these types of errors under consideration here is a function of λ and/or a and, thus, not known a priori. Therefore, they are considered as components to the uncertainty of the measurands.

From a formal point of view, the relevant superscripts, W, L, R, S, P, V, and T, are now replaced by an index J for the subsequent summation:

$$u_B^2(c) = \sum_J u_J^2(c) \tag{53}$$

$$u_B^2(d) = \sum_J u_J^2(d) \tag{54}$$

Table II. Experimental Parameters

Thermal conductivity	$1.14\ \mathrm{W \cdot m^{-1} \cdot K^{-1}}$
Thermal diffusivity	$0.5\ \mathrm{mm \cdot s^{-1}}$
Working temperature	23°C
Rate of heat flow	0.4 W
Wire length	(100 ± 0.5) mm
Wire diameter	(0.175 ± 0.05) mm
Wire heat capacity	$450\ \mathrm{J \cdot kg^{-1} \cdot K^{-1}}$
Wire density	$9000\ \mathrm{kg \cdot m^{-3}}$
Wire temp. coefficient	$(0.006 \pm 0.00005)\ \mathrm{K^{-1}}$
Evaluation time interval	1.2–40 s
Max. temp. excursion	1.9 K
Sampling rate	$14.3\ \mathrm{s^{-1}}$
Current	(1 ± 0.007) A
Voltmeter uncertainty	4×10^{-5} V
Voltmeter integration time	0.017 s
Sample thickness	30 mm
Temperature drift	1×10^{-4} K

Here, $J = 5$, for example, indicates deviations caused by the error P (nonconstant power supply). Using Eqs. (5) and (6), respectively, the standard uncertainties of c and d can be written as follows:

$$u_J(c) = \frac{\sum t_i' \sum \delta U_i^{\mathrm{J}} - N \sum t_i' \, \delta U_i^{\mathrm{J}}}{(\sum t_i')^2 - N \sum t_i'^2} \tag{55}$$

$$u_J(d) = \frac{1}{N} \left(\sum \delta U_i^{\mathrm{J}} - u_j(m) \sum t_i' \right) \tag{56}$$

Equations (55) and (56) complete the set of expressions necessary for assessing the standard uncertainty of the THW method. In accordance with Ref. 7, a typical solution has been derived for values of Pyrex CRM 039 (Certified Reference Material) as listed in Table II. A wire diameter of 0.175 mm has been chosen because this is the most common one in measurements.

First, the B-type variances, u_{B}^2, of slope c and intercept d, introduced by model errors, are determined from Eqs. (55) and (56). The results are given in Table III. Second, introduced by the evaluation procedure, A-type variances, u_{A}^2, of c and d are calculated using the known current source noise for estimating χ^2. According to Eqs. (37) and (38), they follow as

$$(u_{\mathrm{A}}(c)/c)^2 = 9.5 \times 10^{-7} \qquad \text{and} \qquad (u_{\mathrm{A}}(d)/d)^2 = 3.2 \times 10^{-7}$$

Table III. B-Type Variances of Estimation Parameters c and d (cf. Text)

Model error	$(u_J(c)/c)^2$	$(u_J(d)/d)^2$
W	2.5×10^{-5}	1.3×10^{-5}
R	1.6×10^{-5}	2.4×10^{-6}
P	6.0×10^{-4}	4.6×10^{-5}
V	4.8×10^{-6}	2.4×10^{-6}
T	2.3×10^{-5}	1.5×10^{-6}
L	2.9×10^{-6}	5.3×10^{-5}
S	1.1×10^{-7}	8.4×10^{-9}

These values are combined with those given in Table III. The results,

$$(u_c(c)/c)^2 = 6.8 \times 10^{-4} \qquad \text{and} \qquad (u_c(d)/d)^2 = 6.6 \times 10^{-5}$$

are entered into Table IV for subsequent determination of combined variances. Third, the variances for both measurands λ and a from input quantities, x_i, are estimated. The values are listed in Table IV. Inserting the values in Table IV into Eqs. (54) and (55) yields the absolute standard deviations for λ and a, respectively:

$$u(\lambda) = 0.033 \text{ W} \cdot \text{m}^{-1} \cdot \text{K}^{-1} \qquad \text{and} \qquad u(a) = 0.075 \text{ mm}^2 \cdot \text{s}^{-1}$$

The corresponding relative values as percentages are

$$u(\lambda)/\lambda = 2.9\,\% \qquad \text{and} \qquad u(a)/a = 15\,\%$$

Table IV. Variances for Measurands λ and a from Input Quantities, x_i, and Linearization Error

x_i	$(u_{x_i}(\lambda)/\lambda)^2$	$(u_{x_i}(a)/a)^2$
α	7×10^{-5}	—
U_0	1×10^{-8}	—
I	5×10^{-5}	—
L	2.5×10^{-5}	—
r	—	2.5×10^{-3}
c	6.8×10^{-4}	1.7×10^{-2}
d	—	1.7×10^{-3}
Linear model error	2.5×10^{-7}	1.8×10^{-5}

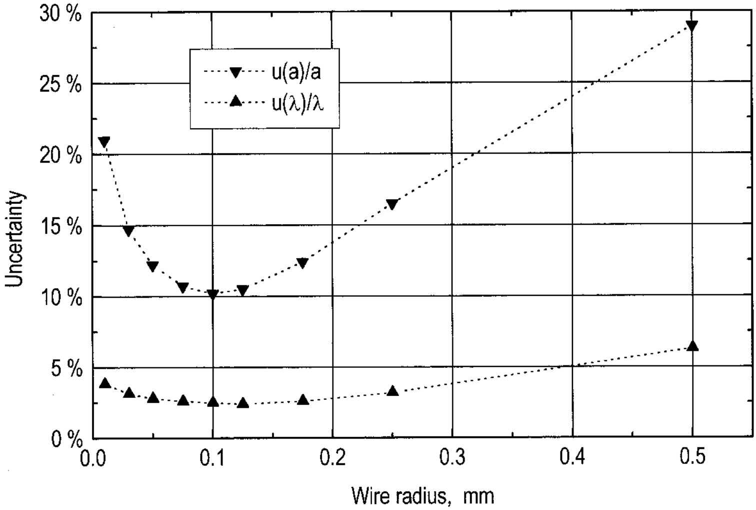

Fig. 9. Uncertainty of thermal conductivity of a Pyrex CRM 039 sample as assessed for wires of different radii (cf. text).

From this, the expanded relative uncertainties for a coverage factor of $k=2$ finally follow:

$$u'(\lambda)/\lambda = 5.8\,\% \qquad \text{and} \qquad u'(a)/a = 30\,\%$$

These values compare with those obtained by the THS technique [6].

Finally, one effect of the (indirect) influence of the wire radius on the uncertainties of thermal conductivity and thermal diffusivity of Pyrex assessed above should be discussed in this section. As plotted in Fig. 9 for different wire radii, both uncertainties first decrease with decreasing wire radius down to a minimum between 0.1 mm and 0.13 mm. But then they increase again. An analysis of the individual uncertainty components shows that at wire radii lower than about 0.15 mm, the error due to the constant current mode (cf. Section 2.4.1) becomes dominant. This is because $\delta U^{\mathrm{P}} \propto \mathrm{Ei}^2(1/\tau^2)$ and $\tau \propto 1/r^2$. Therefore, under conditions as chosen here, THW measurements should be best performed with a wire radius of about 0.1 mm.

4. EXPERIMENTS

As presented in Ref. 6 for the THS method, here, again, the standard uncertainty of the thermal conductivity assessed theoretically is compared with the experimental results obtained from samples of Pyrex 7740 glass.

This material, manufactured by Corning France, was chosen for several reasons: (1) because of its thermal conductivity of $1.14\ W \cdot m^{-1} \cdot K^{-1}$ at room temperature, it represents a wide range of dielectrics; (2) this material has been in use for a long time and has been studied intensively; and (3) our sample was cut from the original bulk that was used for the certification of the standard reference material "CRM 039" for thermal conductivity in which PTB participated [14]. Moreover, our spectral transmittance measurements in the range 1.25 to 20 μm on Pyrex samples of 1-mm thickness show the material to be opaque above 4.7 μm and to have, at room temperature, a total transmittance of only 1.2×10^{-3}. Hence, there should be no significant radiative heat transfer between the wire and the cell walls.

The experiments were performed in the THW standard configuration using a nickel wire 100 mm in length and 0.0875 mm in radius. The dimensions of each sample half are $100 \times 30 \times 18\ mm^3$. The thermal part of the setup is mounted inside our insulated container [6], which is immersed in a thermostated bath. In a four-wire circuit, the wire is connected to a constant current source and a voltmeter. Beginning at time 0, t_0, a constant current of 1 A is passed through the wire for about 2 min, while the voltage drop $U(t_i)$ is recorded pointwise at a sampling rate of $14\ s^{-1}$. For each working temperature T_W, three repeated runs were performed. The maximum departure between the certified values and the results of our experimental runs are 1.4% at most without any systematic deviations (cf. Fig. 10).

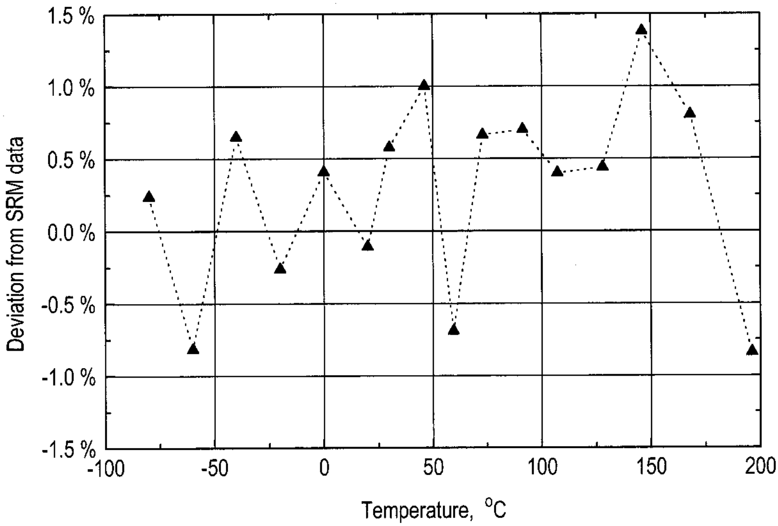

Fig. 10. Deviations between the experimental data and the certified standard data of Pyrex CRM 039.

In Ref. 14 an uncertainty of at least 1.2% is claimed for the SRM data. Hence, the uncertainty values estimated here are in good agreement.

5. SUMMARY

We have assessed the uncertainty of the thermal conductivity and thermal diffusivity for a standard hot wire setup in accordance with the recommendations of the ISO Guide to the Expression of Uncertainty in Measurement [7]. The mathematical model, the evaluation procedure, and the measuring instruments have been analyzed as major uncertainty sources. The expanded uncertainty of 5.8% assessed for λ has been verified experimentally against CRM 039 for temperatures between -75 and 195°C. The deviations of the experimental results from the reference values are within a range of $\pm 1.4\%$ and, hence, confirm the calibration associated with CRM 039 very well.

REFERENCES

1. K. D. Maglic, A. Cezairlyan, and V. E. Peletsky, eds., in *Compendium of Thermophysical Property Measurement Methods, Vol. 1: Survey of Measurement Techniques* (Plenum Press, New York and London, 1984).
2. G. D. Marrow, *Am. Ceram. Soc. Bull.* **58**:687 (1979).
3. Determination of Thermal Conductivity up to 1600°C by the Hot Wire Method, in *DIN 51046* (Beuth Verlag, Berlin, 1973).
4. W. R. Daire and A. Downs, *Trans. Br. Ceram. Soc.* **79**:44 (1980).
5. J. C. Willshee, *Proc. Br. Ceram. Soc.* **29**:153 (1980).
6. U. Hammerschmidt and W. Sabuga, *Int. J. Thermophys.* **21**:217 (2000).
7. *Guide to the Expression of Uncertainty in Measurement* (ISO, Geneva, 1992).
8. J. J. Healy, J. J. de Groot, and J. Kestin, *Physica* **82C**:392 (1976).
9. R. Siegel and J. R. Howell, in *Thermal Radiation Heat Transfer*, 2nd ed. (Hemisphere, Washington, DC, 1981).
10. J. H. Blackwell, *Can. J. Phys.* **31**:472 (1953).
11. J. H. Blackwell, *Can. J. Phys.* **34**:412 (1956).
12. W. T. Kierkus, N. Mani, and J. E. S. Venart, *Can. J. Phys.* **51**:1182 (1973).
13. H. Tautz, in *Wärmeleitung und Temperaturausgleich* (Verlag Chemie GmbH, Weinheim, 1971).
14. I. Williams and R. E. Shawyer, Certification report for a Pyrex glass reference material for thermal conductivity between -80°C and 200°C (CRM 039). BCR Information Reference Materials, Report EUR 13358 (1991).